Contents lists available at ScienceDirect

Nuclear Inst. and Methods in Physics Research, B

A fitting algorithm for optimizing ion implantation energies and fluences

Pauli Kehayias [a,*], Jacob Henshaw [b], Maziar Saleh Ziabari [b,c], Michael Titze [a], Edward Bielejec [a], Michael P. Lilly [b], Andrew M. Mounce [b]

[a] *Sandia National Laboratories, Albuquerque, New Mexico 87185, USA*
[b] *Center for Integrated Nanotechnologies, Sandia National Laboratories, Albuquerque, New Mexico 87123, USA*
[c] *University of New Mexico Department of Physics and Astronomy, Albuquerque, New Mexico 87131, USA*

ARTICLE INFO

ABSTRACT

We describe a method to automatically generate an ion implantation recipe, a set of energies and fluences, to produce a desired defect density profile in a solid using the fewest required energies. We simulate defect density profiles for a range of ion energies, fit them with an appropriate function, and interpolate to yield defect density profiles at arbitrary ion energies. Given N energies, we then optimize a set of N energy-fluence pairs to match a given target defect density profile. Finally, we find the minimum N such that the error between the target defect density profile and the defect density profile generated by the N energy-fluence pairs is less than a given threshold. Inspired by quantum sensing applications with nitrogen-vacancy centers in diamond, we apply our technique to calculate optimal ion implantation recipes to create uniform-density 1 μm surface layers of ^{15}N or vacancies (using ^{4}He).

1. Introduction

Ion implantation and irradiation are critical techniques with multiple application areas. These include the formation of dopant layers in semiconductor devices [1] and the creation of defect centers in diamond and other wide-bandgap materials for quantum optics and sensing, electron and hole dopants to alter the conductivity, and graphitization to make electrical contacts and membranes [2–7]. Other examples include making uniform damage layers to alter the superconducting critical temperature T_c in YBaCuO films [8] and to enable high-resolution diamond cutting [9], to name a few. While knowing the implanted ion range and straggle for a given energy is important in these highlighted examples, there are many instances where a single-energy ion implantation cannot produce the desired ion or vacancy distribution in a material, including in the examples referenced above. For these types of applications, the community typically uses Stopping Range of Ions in Matter (SRIM) simulations to predict the ion density and vacancy density depth distributions for ion implantations into solids [10]. However, manually calculating and choosing a set of implantation energies and fluences (ions/cm^2) to satisfactorily match a desired defect density profile can be laborious and inaccurate, especially as the number of required implants increases.

In this paper, we describe a method to computationally generate ion implantation recipes for arbitrary defect density profiles using least-squares curve fitting. We do this by fitting a set of simulated defect density profiles from SRIM, interpolating the resulting fit parameters, and minimizing the number of ion implantation energy-fluence pairs required to produce a recipe that closely matches the desired defect density profile.

We are motivated by the past success using SRIM simulations to calculate the ion implantation recipes to make shallow layers of nitrogen-vacancy (NV) defect centers in diamond, which are used for sensing magnetic sources external to the diamond surface [11–13]. An NV center consists of a substitutional nitrogen atom in the diamond lattice adjacent to a vacancy. To create a surface layer of NV centers, one can implant nitrogen into a diamond sample with few-ppb impurity density (which also creates vacancies) or implant another ion (such as helium) into a diamond sample with nitrogen defects (~100 ppm) to create vacancies. The resulting NV layer distribution is expected to match that of the implanted nitrogen or vacancy density, though a full treatment should also include vacancy–interstitial recombination and other corrections. Since the magnetic field amplitude that an NV center senses depends on the distance to the magnetic source (such as a magnetic dipole), tailoring the NV layer thickness and depth is important to optimize the magnetic signal-to-noise ratio. By predicting the implantation characteristics using SRIM, we engineer an ideal NV layer to suit our magnetometry specifications.

---

* Corresponding author.
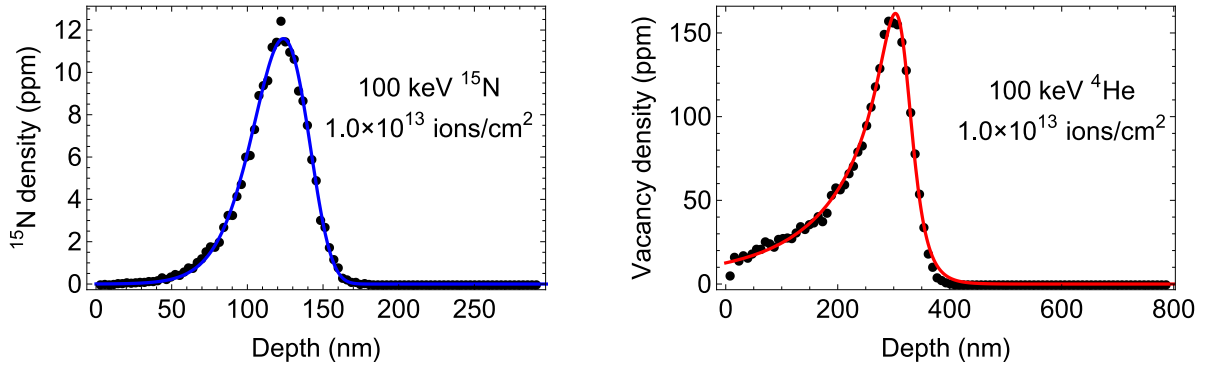 *E-mail address:* pmkehay@sandia.gov (P. Kehayias).

Fig. 1. (Left) Simulated ^{15}N density $\rho_{\text{sim}}(z)$ (black) and $\rho_{\text{Gaus}}(z)$ fit (blue). (Right) Simulated ^{4}He-induced vacancy density $\rho_{\text{sim}}(z)$ (black) and $\rho_{\text{Lor}}(z)$ fit (red). The vacancy density is the sum of the vacancies created by the ^{4}He ions and the vacancies created by carbon recoils. For diamond, 1 ppm $= 1.76 \times 10^{17}$ atoms/cm^3. The systematic residuals are small (<1% of the maximum) compared to the statistical residuals (about 2% of the maximum). (For interpretation of the references to color in this figure caption, the reader is referred to the web version of this article.)

2. Methods

Our ion implantation recipe optimization algorithm consists of the following steps:

1. Simulate ion implantation defect density profiles for a list of ion energies using SRIM.
2. Fit the resulting defect density profile using an empirical fit function, then interpolate the fit parameters as a function of energy.
3. For a given number of ion implantation energies N, calculate the ion implantation recipe (energy-fluence pairs) that best fits to the target defect density profile.
4. Repeat step 3 with increasing N until the ion implantation recipe produces a defect density profile that resembles the target defect density profile within a given error limit.

We applied this algorithm to two situations relevant to creating shallow NV layers in diamond for magnetic sensing and imaging of near-surface external magnetic sources [2,3]. In the first example, we calculated the implantation recipe needed to create a flat-top ^{15}N density in a diamond substrate (few-ppb impurity density) with a 1 μm thickness (similar to Sample B in Ref. [14]). In the second example, we calculated the ^{4}He implant recipe needed to create a 1 μm uniform layer of vacancies in a diamond substrate. In this recipe, the diamond substrate already has an appreciable nitrogen density in the bulk (~100 ppm), and we implant with ^{4}He to create vacancies and convert nitrogen defects to NV defects [12,13].

2.1. Ion implantation and defect density profile simulations

We simulated ^{15}N and ^{4}He ion implants using the SRIM Monte Carlo simulation software and the `pysrim` Python library [10,15]. For each ion, we first generated the projected range and longitudinal straggle as a function of energy using the Projected Range Algorithm (PRAL) included as part of the SRIM software package [10,16]. This enabled us to assign an appropriate depth range for the transport of ions in matter (TRIM) simulation, which produced the defect density profiles used in later steps. For ^{15}N we simulated 58 energies spanning from 10 keV to 1500 keV (15 nm to 960 nm in depth), and for ^{4}He we simulated 63 energies spanning from 5 keV to 1500 keV (22 nm to 2550 nm in depth).

For each energy, we used quick TRIM to simulate 10,000 ions incident at 8° from the diamond surface normal (usually the [100] crystallographic axis) to avoid channeling along crystallographic axes in real diamond samples. The diamond substrate was modeled as a ^{12}C solid with 3.51 g/cm^3 density, 37.5 eV atom displacement threshold energy, 3 eV lattice damage threshold, and 7.4 eV surface damage threshold [17–20]. Each simulation calculated the ion and vacancy densities for 100 evenly-spaced depth bins starting from the surface, and we expanded the depth spacing (and overall depth) with increasing ion energy. Fig. 1 shows example defect density profiles for ^{15}N and ^{4}He implants (100 keV, 1.0×10^{13} ions/cm^2).

2.2. Defect density profile fitting

For each implantation energy, we fit the simulated defect density profile $\rho_{\text{sim}}(z)$ as a function of depth z using an asymmetric Gaussian (Lorentzian) distribution for ions (vacancies), defined as [21]

$$\rho_{\text{Gaus}}(z) = \frac{A(1 + e^{a(z-z_0)})^2}{4} \exp\left[-\frac{(1 + e^{a(z-z_0)})^2}{4}\frac{(z - z_0)^2}{2\sigma^2}\right], \qquad (1)$$

$$\rho_{\text{Lor}}(z) = \frac{A\sigma^2}{\sigma^2 + \frac{(1+e^{a(z-z_0)})^2}{4}(z - z_0)^2}. \qquad (2)$$

In these expressions, z_0 is a depth with maximum defect density, σ is a linewidth, A is a maximum amplitude, and a is an asymmetry parameter ($a = 0$ corresponds to no asymmetry). Fig. 1 shows the asymmetric Gaussian and Lorentzian fits used for two example $\rho_{\text{sim}}(z)$ distributions; while these fit functions are empirical, they are able to capture the simulated lineshapes well. The fit functions smooth out the statistical noise in $\rho_{\text{sim}}(z)$ and generate a continuous function for each defect density profile. After fitting each $\rho_{\text{sim}}(z)$ for our simulation range, we interpolate z_0, σ, A, and a as a function of energy (Fig. 2) to yield the defect density profile for any energy within the simulated range.

2.3. Ion implantation energy and fluence optimization

For a set of N energies and fluences in an ion implantation recipe, the total defect density profile is

$$\rho_{\text{recipe}}(z, N) = \sum_{i=1}^{N} f_i \rho_{E_i}(z) . \qquad (3)$$

Here, E_i is the energy for the i'th ion implant, f_i is the fluence, and $\rho_{E_i}(z)$ is the defect density profile for the i'th ion implant and energy ($\rho_{\text{Gaus}}(z)$ or $\rho_{\text{Lor}}(z)$ with interpolated $\{z_0, \sigma, A, a\}$ parameters). For a given N, we perform a least-squares fit, which automatically minimizes $\int_0^\infty \left[\rho_{\text{recipe}}(z, N) - \rho_{\text{target}}(z)\right]^2 dz$ to yield a set of N $\{E_i, f_i\}$ pairs.

2.4. Finding the number of implants to meet the error limit

Finally, we find the minimum number of energies such that the percent error (Δ) between $\rho_{\text{recipe}}(z, N)$ and $\rho_{\text{target}}(z)$ is less than a chosen threshold, where Δ (evaluated numerically) is defined as:

$$\Delta = \frac{\int_0^\infty |\rho_{\text{recipe}}(z, N) - \rho_{\text{target}}(z)| \, dz}{\int_0^\infty \rho_{\text{target}}(z) \, dz} \times 100\% . \qquad (4)$$
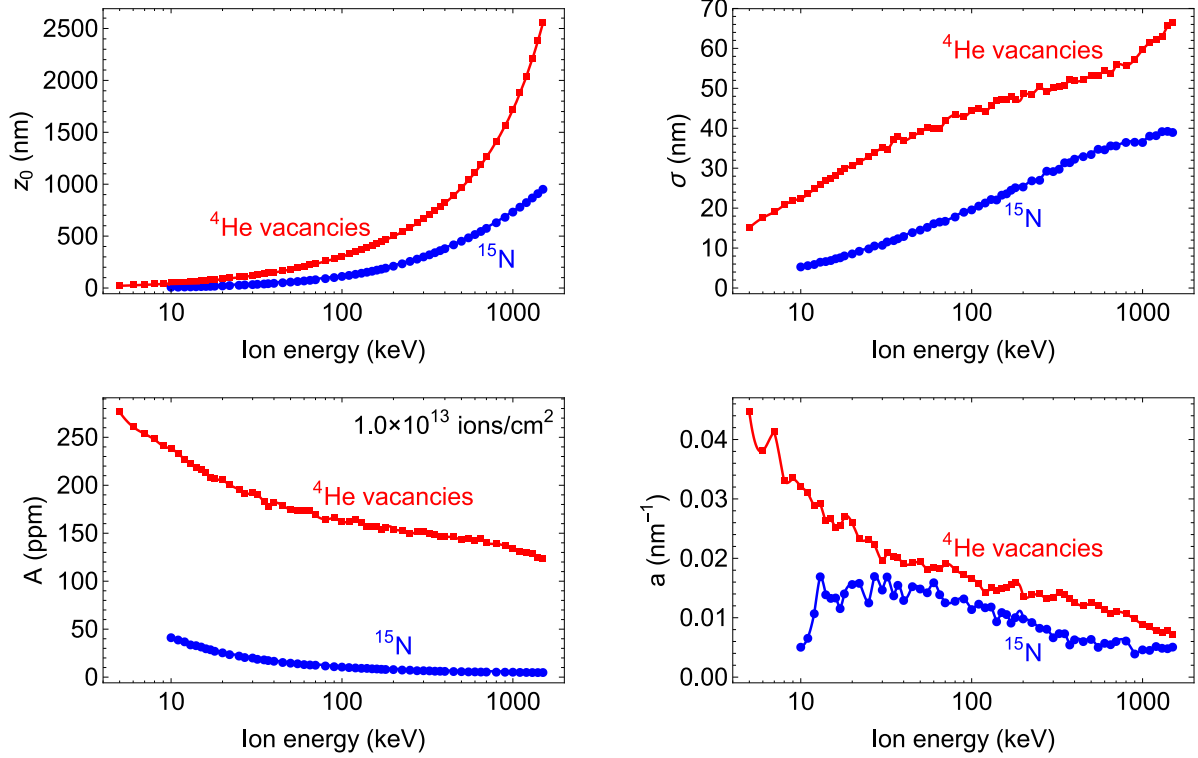
Fig. 2. Extracted z_0, σ, A, and a parameters for the ^{15}N asymmetric Gaussian fits (blue) and ^{4}He vacancy asymmetric Lorentzian fits (red). Here we assume a 1.0×10^{13}/cm^2 fluence for each. (For interpretation of the references to color in this figure caption, the reader is referred to the web version of this article.)

Table 1

Calculated ^{15}N and ^{4}He implant energies and fluences for a 1 μm 50 ppm defect layer, also shown in Fig. 3.

^{15}N energy (keV)	^{15}N fluence (ions/cm^2)	^{4}He energy (keV)	^{4}He fluence (ions/cm^2)
10	1.3E13	8	1.2E12
25	2.0E13	23	1.4E12
48	2.8E13	47	1.6E12
79	3.4E13	80	1.8E12
120	4.0E13	121	1.8E12
170	4.8E13	170	1.9E12
229	5.2E13	227	2.0E12
299	5.9E13	288	2.0E12
384	6.4E13	354	2.1E12
483	6.6E13	422	2.2E12
599	7.0E13	494	3.8E12
734	7.4E13		
891	7.7E13		
1064	7.6E13		
1255	7.9E13		
1478	9.8E13		

density profile as:

$$\rho_{\text{target}}(z) = \begin{cases} 50 \text{ ppm} & \text{for } 0 \text{ nm} \leq z \leq 1000 \text{ nm}, \\ 0 \text{ ppm} & \text{for } 1000 \text{ nm} < z \leq 1300 \text{ nm}. \end{cases} \tag{5}$$

Fig. 3a–b shows the defect density profiles generated by applying the above algorithm. We find that a minimum of sixteen ^{15}N implants and eleven ^{4}He implants are required to achieve $\Delta < 10\%$. Table 1 lists the energies and fluences for each fit in Fig. 3. For both ^{15}N and ^{4}He optimizations, Δ converges to about 3%. This is because for shallow z, we become limited by the lineshape of the shallowest simulated implant. With increasing N, the fitting algorithm reduces E_1 (the energy of the lowest-energy implant) until E_1 equals the minimum available ion energy. In addition, the fit becomes overparameterized for sufficiently large N, which is realized when the fit yields duplicate energies or fluences that are approximately zero.

4. Conclusions and outlook

In this work, we described a way to empirically fit the simulated defect density profiles simulated by SRIM, predict the expected defect density profile for any energy within the simulated range, and calculate the ideal set of energies and fluences for a desired defect density profile (such as a uniform flat-top surface layer). By doing these steps computationally with least-squares fitting, we avoid having to guess the necessary implant parameters to formulate the implant recipe. This method is generalizable to other situations, such as calculating non-uniform defect densities to compensate for depth-dependent NV conversion efficiency and coherence time [22–24], and also to creating defect layers with other ions and solids. After implanting diamond samples with ^{15}N based on this algorithm and annealing to improve the NV yield, we were able to produce diamond samples with ~1 μm NV surface layers to use for NV magnetic microscopy applications [25,26]. The results of this work can be validated using techniques such as confocal microscopy or secondary-ion mass spectrometry (SIMS).
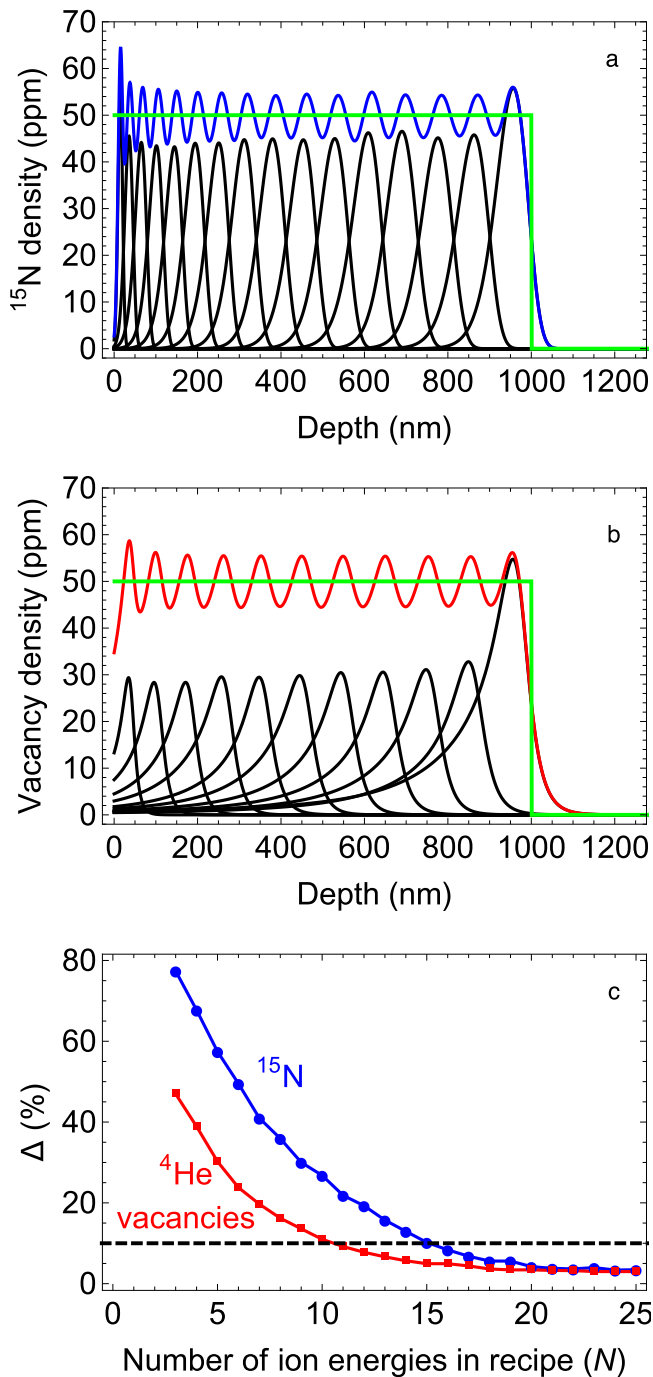
Although increasing N typically decreases Δ, this also adds more implantation steps and cost. To avoid generating unnecessarily complicated ion implantation recipes, we find the smallest N for which the Δ discrepancy is satisfactory. For a given N we perform a least-squares fit for the set of $\{E_i, f_i\}$ energies and fluences, compare to a desired threshold Δ_{th} (for example, $\Delta_{\text{th}} = 10\%$), and repeat with increasing N until we fulfill our $\Delta \leq \Delta_{\text{th}}$ requirement.

3. Results and discussion

In order to make an NV surface-layer diamond sample ideal for magnetically sensing external sources ~1–10 μm away from the surface, we want to create an implant recipe that has a uniform 50 ppm ^{15}N or vacancy density and a 1 μm thickness. We define this target defect

Fig. 3. Fitted $\rho_{recipe}(z, N)$ defect density profiles for a 1 μm 50 ppm flat-top for ^{15}N (a) and ^{4}He-induced vacancies (b). The black curves represent the defect density profiles from the constituent implants, which sum to approximate a uniform flat-top density $\rho_{target}(z)$ (green). (c) Percent error between $\rho_{target}(z)$ and $\rho_{recipe}(z, N)$ for an increasing number of energies N. The dashed line indicates $\Delta_{th} = 10\%$, which is the threshold we use for this work. (For interpretation of the references to color in this figure caption, the reader is referred to the web version of this article.)

Our simulations and analysis currently do not include effects from defect diffusion during annealing, vacancy–interstitial recombination after implantation and after annealing, NV conversion efficiency as a function of depth, or ion channeling along crystallographic axes [27–30]. Depending on the importance for a given application, one may implement these corrections either at the SRIM simulation stage, as adjustments to the $\rho_{sim}(z)$ or $\rho_{E_i}(z)$ defect density profiles, or by modifying $\rho_{target}(z)$.

CRediT authorship contribution statement

Declaration of competing interest

The authors declare that they have no known competing financial interests or personal relationships that could have appeared to influence the work reported in this paper.

Acknowledgments

References

[1] J.D. Plummer, M.D. Deal, P.B. Griffin, Silicon VLSI Technology: Fundamentals, Practice and Modeling, Prentice Hall, 2000.

[2] J.R. Rabeau, P. Reichart, G. Tamanyan, D.N. Jamieson, S. Prawer, F. Jelezko, T. Gaebel, I. Popa, M. Domhan, J. Wrachtrup, Implantation of labelled single nitrogen vacancy centers in diamond using ^{15}N, Appl. Phys. Lett. 88 (2) (2006) 023113.

[3] J. Achard, V. Jacques, A. Tallaire, Chemical vapour deposition diamond single crystals with nitrogen-vacancy centres: a review of material synthesis and technology for quantum sensing applications, J. Phys. D: Appl. Phys. 53 (31) (2020) 313001.

[4] Rafi Kalish, Ion-implantation in diamond and diamond films: doping, damage effects and their applications, Appl. Surf. Sci. 117–118 (1997) 558–569.

[5] F. Fontaine, C. Uzan-Saguy, B. Philosoph, R. Kalish, Boron implantation/in situ annealing procedure for optimal p-type properties of diamond, Appl. Phys. Lett. 68 (16) (1996) 2264–2266.

[6] M. De Feudis, V. Mille, A. Valentin, O. Brinza, A. Tallaire, A. Tardieu, R. Issaoui, J. Achard, Ohmic graphite-metal contacts on oxygen-terminated lightly boron-doped CVD monocrystalline diamond, Diam. Relat. Mater. 92 (2019) 18–24.

[7] Jonathan C. Lee, Andrew P. Magyar, David O. Bracher, Igor Aharonovich, Evelyn L. Hu, Fabrication of thin diamond membranes for photonic applications, Diam. Relat. Mater. 33 (2013) 45–48.

[8] U. Barkow, D. Menzel, S.S. Tinchev, Creating homogeneous depth profiles in YBaCuO films by ion beam implantation for uniform suppression of T_c, Physica C: Superconductivity 370 (4) (2002) 246–252.

[9] Jinshi Wang, Xiaodong Zhang, Fengzhou Fang, Rongtai Chen, Diamond cutting of micro-structure array on brittle material assisted by multi-ion implantation, Int. J. Mach. Tools Manuf. 137 (2019) 58–66.

[10] James F. Ziegler, M.D. Ziegler, J.P. Biersack, SRIM – the stopping and range of ions in matter (2010), Nucl. Instrum. Methods Phys. Res. B 268 (11) (2010) 1818–1823, 19th International Conference on Ion Beam Analysis.

[11] P. Kehayias, A. Jarmola, N. Mosavian, I. Fescenko, F.M. Benito, A. Laraoui, J. Smits, L. Bougas, D. Budker, A. Neumann, S.R.J. Brueck, V.M. Acosta, Solution nuclear magnetic resonance spectroscopy on a nanostructured diamond chip, Nature Commun. 8 (1) (2017) 188.

[12] Ilja Fescenko, Abdelghani Laraoui, Janis Smits, Nazanin Mosavian, Pauli Kehayias, Jong Seto, Lykourgos Bougas, Andrey Jarmola, Victor M. Acosta, Diamond Magnetic Microscopy of Malarial Hemozoin Nanocrystals, Phys. Rev. Appl. 11 (2019) 034029.

[13] Ed E. Kleinsasser, Matthew M. Stanfield, Jannel K.Q. Banks, Zhouyang Zhu, Wen-Di Li, Victor M. Acosta, Hideyuki Watanabe, Kohei M. Itoh, Kai-Mei C. Fu, High density nitrogen-vacancy sensing surface created via He$^+$ ion implantation of ^{12}C diamond, Appl. Phys. Lett. 108 (20) (2016).

[14] Pauli Kehayias, Ezra Bussmann, Tzu-Ming Lu, Andrew M. Mounce, A physically unclonable function using NV diamond magnetometry and micromagnet arrays, J. Appl. Phys. 127 (20) (2020) 203904.

[15] Christopher Ostrouchov, Yanwen Zhang, William J. Weber, pysrim: Automation, Analysis, and Plotting of SRIM Calculations, Journal of Open Source Software 3 (28) (2018) 829.

[16] J.P. Biersack, Calculation of projected ranges — analytical solutions and a simple general algorithm, Nucl. Instrum. Methods 182–183 (1981) 199–206.

[17] James F. Ziegler, Jochen P. Biersack, Matthias D. Ziegler, SRIM: The Stopping and Range of Ions in Matter, 2008.

[18] J. Koike, D.M. Parkin, T.E. Mitchell, Displacement threshold energy for type IIa diamond, Appl. Phys. Lett. 60 (12) (1992) 1450–1452.

[19] Michael Hoch, Paul E. Blackburn, David P. Dingledy, Herrick L. Johnston, The Heat of Sublimation of Carbon, J. Phys. Chem. 59 (2) (1955) 97–99.

[20] Daniel V. Schroeder, An Introduction To Thermal Physics, Addison Wesley Longman, 2000.

[21] Aaron L. Stancik, Eric B. Brauns, A simple asymmetric lineshape for fitting infrared absorption spectra, Vib. Spectrosc. 47 (1) (2008) 66–69.

[22] S. Pezzagna, B. Naydenov, F. Jelezko, J. Wrachtrup, J. Meijer, Creation efficiency of nitrogen-vacancy centres in diamond, New J. Phys. 12 (6) (2010) 065017.

[23] J. Schwartz, S. Aloni, D.F. Ogletree, M. Tomut, M. Bender, D. Severin, C. Trautmann, I.W. Rangelow, T. Schenkel, Local formation of nitrogen-vacancy centers in diamond by swift heavy ions, J. Appl. Phys. 116 (21) (2014) 214107.

[24] B.A. Myers, A. Das, M.C. Dartiailh, K. Ohno, D.D. Awschalom, A.C. Bleszynski Jayich, Probing Surface Noise with Depth-Calibrated Spins in Diamond, Phys. Rev. Lett. 113 (2014) 027602.

[25] D.R. Glenn, R.R. Fu, P. Kehayias, D. Le Sage, E.A. Lima, B.P. Weiss, R.L. Walsworth, Micrometer-scale magnetic imaging of geological samples using a quantum diamond microscope, Geochem. Geophys. Geosyst. 18 (8) (2017) 3254–3267.

[26] Edlyn V. Levine, Matthew J. Turner, Pauli Kehayias, Connor A. Hart, Nicholas Langellier, Raisa Trubko, David R. Glenn, Roger R. Fu, Ronald L. Walsworth, Principles and techniques of the quantum diamond microscope, Nanophotonics 8 (11) (2019) 1945–1973.

[27] D. Antonov, T. Häussermann, A. Aird, J. Roth, H.-R. Trebin, C. Müller, L. McGuinness, F. Jelezko, T. Yamamoto, J. Isoya, S. Pezzagna, J. Meijer, J. Wrachtrup, Statistical investigations on nitrogen-vacancy center creation, Appl. Phys. Lett. 104 (1) (2014) –.

[28] Hisashi Sumikura, Kazuyuki Hirama, Katsuhiko Nishiguchi, Akihiko Shinya, Masaya Notomi, Highly nitrogen-vacancy doped diamond nanostructures fabricated by ion implantation and optimum annealing, APL Mater. 8 (3) (2020) 031113.

[29] J.O. Orwa, K. Ganesan, J. Newnham, C. Santori, P. Barclay, K.M.C. Fu, R.G. Beausoleil, I. Aharonovich, B.A. Fairchild, P. Olivero, A.D. Greentree, S. Prawer, An upper limit on the lateral vacancy diffusion length in diamond, Diam. Relat. Mater. 24 (2012) 6–10.

[30] M. Posselt, J.P. Biersack, Computer simulation of ion implantation into crystalline targets, Nucl. Instrum. Methods Phys. Res. B 64 (1) (1992) 706–710.

[31] Example Python analysis code and SRIM simulation data are available for download from https://github.com/dangernoodle-dev/srimfit.